Biosensors and Bioelectronics 64 (2015) 499–504

Contents lists available at ScienceDirect

Biosensors and Bioelectronics

journal homepage: www.elsevier.com/locate/bios

Enhanced photoelectrochemical property of ZnO nanorods array synthesized on reduced graphene oxide for self-powered biosensing application

Zhuo Kang [a], Yousong Gu [a], Xiaoqin Yan [a], Zhiming Bai [a], Yichong Liu [a], Shuo Liu [a], Xiaohui Zhang [a], Zheng Zhang [a], Xueji Zhang [b], Yue Zhang [a,c,*]

[a] State Key Laboratory for Advanced Metals and Materials, School of Materials Science and Engineering, University of Science and Technology Beijing, Beijing 100083, China
[b] Research Center for Bioengineering and Sensing Technology, School of Chemistry and Biological Engineering, University of Science and Technology Beijing, Beijing 100083, China
[c] Key Laboratory of New Energy Materials and Technologies, University of Science and Technology Beijing, Beijing 100083, China

ARTICLE INFO

Article history:
Received 16 July 2014
Received in revised form
2 September 2014
Accepted 22 September 2014
Available online 28 September 2014

Keywords:
Photoelectrochemical biosensor
Reduced graphene oxide
ZnO nanorods array
Glutathione
Photoresponse

ABSTRACT

We have realized the direct synthesis of ZnO nanorods (ZnO NRs) array on reduced graphene layer (rGO), and demonstrated the enhanced photoelectrochemical (PEC) property of the rGO/ZnO based photoanode under UV irradiation compared with the pristine ZnO NRs array. The introduction of the rGO layer resulted in a favorable energy band structure for electron migration, which finally led to the efficient photoinduced charge separation. Such nanostructure was subsequently employed for self-powered PEC biosensing of glutathione in the condition of 0 V bias, with a linear range from 10 to 200 μM, a detection limit of 2.17 μM, as well as excellent selectivity, reproducibility and stability. The results indicated the rGO/ZnO nanostructure is a competitive candidate in the PEC biosensing field.

1. Introduction

In recent years, there has been significant interest in fabricating photoelectrochemical (PEC) biosensors, which are highly promising for bioanalysis owing to their desirable biosensing performance. Since the excitation source (light) and detection signal (photocurrent) are completely separated, such PEC biosensing measurement technique acquire efficient reduction of undesired background noise and improved sensitivity (Liang et al., 2008; Yan et al., 2014). So far, much related research is focused on enhancement of the PEC biosensor performance by incorporating numerous functional nanomaterials, such as traditional metal oxide semiconductors like ZnO (Li et al., 2014; Liu et al., 2014; Zhan et al., 2013), Cu_2O (Li et al., 2014) and TiO_2 (Chen et al., 2012; Tang et al., 2014; Yan et al., 2014), quantum dots like CdS (Zhao et al., 2012) and CdSe (Yan et al., 2014; Zhang et al., 2011), as well as graphene (Hu et al., 2013; Zhang et al., 2011; Zhao et al., 2012). More specifically, IrO_2–Hemin–TiO_2 nanowire arrays (Tang et al., 2013) and Cu_2O/ZnO nanorod array heterostructure (Li et al., 2014) were prepared for sensitive detection of glutathione. Besides, ZnO@ZIF-8 nanorods core–shell heterostructure was applied for selective response toward H_2O_2 (Zhan et al., 2013). And ZnO–Graphene–S6 aptamers photoanode was adopted for PEC detection of SK-BR-3 breast cancer cells (Liu et al., 2014). More recently, DNA-CdSe/TiO_2 film (Yan et al., 2014) and bismuthoxyiodide nanoflakes/TiO_2 nanotubes array based p–n heterojunction (Zhao et al., 2014) were constructed for sensing o-aminophenol and glucose, respectively. However, it is still a challenge to exploit novel approaches for PEC detection of biomolecules with enhanced performance.

ZnO nanomaterials have been intensively studied as a practically applicable component in photoelectric devices and photovoltaic cells due to its direct band gap of 3.37 eV, relatively large exciton binding energy (60 meV), rather rich morphology world and stability against photocorrosion (Zhang et al., 2012). Moreover, the typical electron mobility in ZnO is 10–100 folds higher than TiO_2, who has similar bandgap and band edge positions as ZnO (Hendry et al., 2006; Kaidashev et al., 2003; Yang et al., 2009a, 2009b). Neverthless, we still need to retard the quick

* Corresponding author at: University of Science and Technology Beijing, School of Materials Science and Engineering, State Key Laboratory for Advanced Metals and Materials, 30 Xueyuan Road, Haidian District, Beijing 100083, China. Fax: +86 10 62333113.
E-mail address: yuezhang@ustb.edu.cn (Y. Zhang).

http://dx.doi.org/10.1016/j.bios.2014.09.055
0956-5663/

recombination of photoinduced electron–hole pairs in order to improve the PEC performance of ZnO in aqueous solution. A particularly effective method to solve such a problem is to modify ZnO to acquire the hybrid nanostructure. The controlled growth of ZnO nanostructures on graphene has already received considerable attention (Chang et al., 2011; Choi et al., 2011; Kumar et al., 2011; Liu et al., 2013; Yue et al., 2014), and was subsequently applied for piezoelectric nanogenerators (Kumar et al., 2011), UV sensors (Chang et al., 2011; Liu et al., 2013) and electrochemical biosensors (Yue et al., 2014).

In this work, we demonstrated for the first time the development of a self-powered, UV-activated PEC biosensor based on vertical ZnO nanorods (NRs) array directly synthesized on graphene with suitable energy band alignment (Liu et al., 2014, 2013). In the heterostructure, ZnO NRs array functioned as UV absorbing and charge carrier generating materials, while graphene layer acted as an excellent conductive matrix due to the high electron mobility (15,000 $cm^2 V^{-1} s^{-1}$) (Geim and Novoselov, 2007). This significantly facilitated the photogenerated electron migration to the electrode and efficiently strengthened the charge separation (Chang et al., 2011; Liu et al., 2014; Zhao et al., 2012), finally resulting in the enhanced PEC property. On the basis of this, such heterostructure was further adopted as a PEC biosensing platform for detection of glutathione (GSH) at bias of 0 V, with a rapid response, relatively wide concentration range, low detection limit as well as good selectivity and stability. The rGO/ZnO NRs array provided a robust approach for UV PEC detection of biomolecules.

2. Experimental section

2.1. Materials and reagents

rGO was purchased from Pula Nanotech Ltd. (Tianjin, PR China). GSH, ascorbic acid (AA), uric acid (UA), lactic acid (LA), dopamine, glucose, bovine serum albumin (BSA), and glycine (Gly) were purchased from Sigma-Aldrich. 0.1 M pH 7.4 phosphate buffer saline (PBS) was always employed as the supporting electrolyte. Other reagents were of analytical grade and all aqueous solutions were prepared with deionized water.

2.2. Apparatus

The samples were characterized by Field emission scanning electron microscopy (FESEM, Zeiss, SUPRA-55, German), transmission electron microscopy (TEM, JEOL, JEM-100CX II, Japan), Raman spectrometer (Jobin-Yvon, JY-HR800, 514 nm), and X-ray diffractometer (XRD, Rigaku DMAX-RB, Japan CuKα). The composition of samples was analyzed by X-ray photo-electron spectroscopy (XPS, Axis UltraDLD, SHIMADZU, Japan). The binding energies were normalized to the signal for adventitious carbon at 284.8 eV. The UV irradiation was provided by a UV lamp (Spectronics-L980683) emitting at 365 nm with a power density of 1 mW/cm^2.

2.3. Preparation of rGO/ZnO based photoanode

The rGO ethyl alcohol dispersion (1 mg/ml, 10 μL) was first spin-coated onto the surface of FTO to form a thin and uniform layer and dried at 4 °C for 12 h (Zhang et al., 2014). Then, the rGO film was adopted as the platform for the growth of ZnO NRs array through hydrothermal method. For seed-supported synthesis of ZnO, the ZnO seed layer was acquired by spin coating a colloidal solution of zinc acetate [$Zn(CH_3CO_2)_2$] (0.05 M) onto the rGO layer, and subsequently annealed at 350 °C in N_2 for 5 min. In the hydrothermal process, Zinc nitrate hexahydrate [$Zn(NO_3)_2 \cdot 6H_2O$] and hexamethylenetetramine (HMTA) [$(CH_2)_6N_4$] were dissolved in deionized (DI) water with equal concentration of 50 mM. In addition, polyetherimide (PEI) (5 mM) was dissolved in the solution to enhance the aspect ratio of the NRs array. Subsequently, the substrate was placed in the precursor solution at 90 °C for 3 h, and then rinsed with DI water for three times.

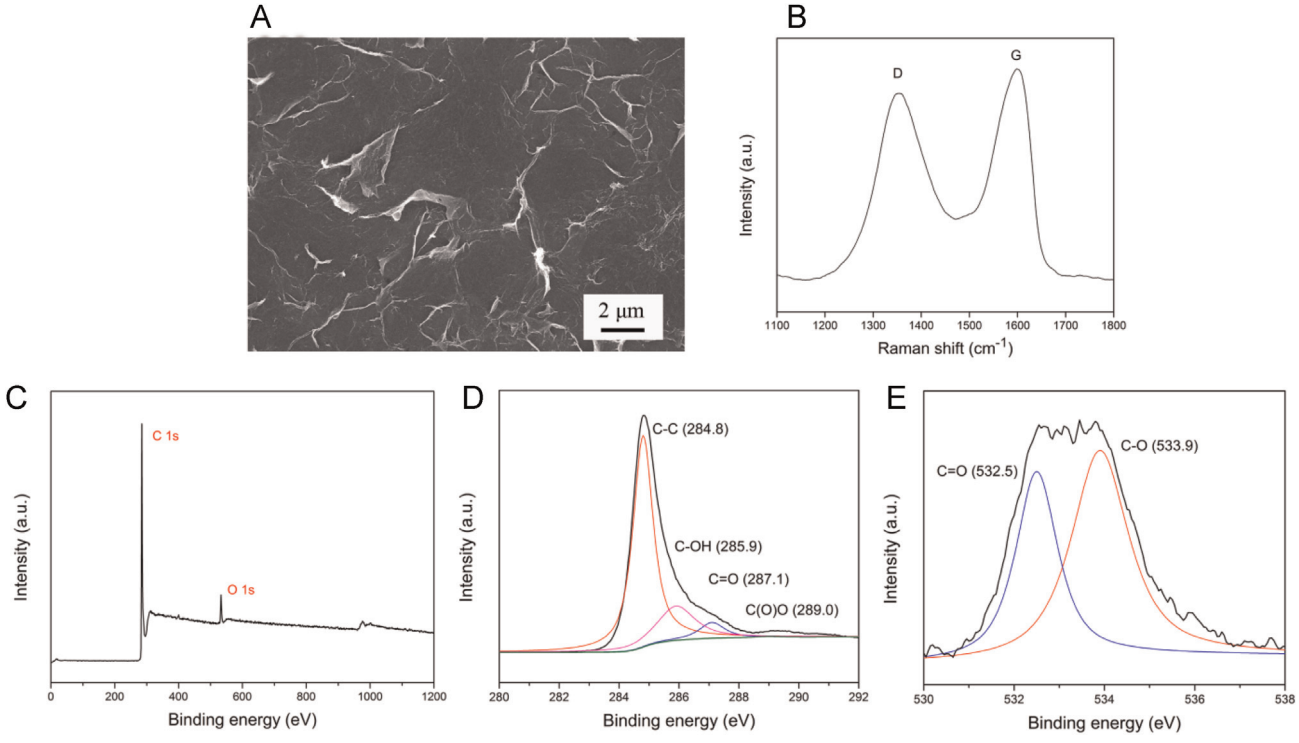

Fig. 1. Characterization of rGO. (A) FE-SEM image of the spin-coating rGO layer; (B) Raman spectra of rGO at excitation wavelength of 514 nm; XPS spectra of rGO: (C) wide scan; (D) C1s; (E) O1s.

3. Results and discussion

3.1. Characterization of rGO layer

Fig. 1A shows the image of the obtained graphene layer. The well-defined D and G bands of graphene can be observed in Raman spectra (Fig. 1B). The doubly degenerate zone center E2g mode G peak located at $\sim$1580 cm^{-1} while the first order scattering from zone boundary phonon D band at $\sim$1350 cm^{-1}. The relative ratio of D and G band intensity (I_D/I_G) was 0.885, revealing numerous defects contained in the sample. Further investigation of the graphene layer by XPS was carried out and the result is presented in Fig. 1C–E. The wide scan XPS spectrum of the graphene sample (Fig. 1C) confirmed the existence of carbon and oxygen elements without other impurity elements. For C1s (Fig. 1D), the C–C bond located at 284.8 eV, compared to which, the peak intensities of C–OH (285.9 eV), C=O (287.1 eV) and C(O)O (289.0 eV) (Fan et al., 2010; Zhang et al., 2013; Yang et al., 2009a, 2009b) were very weak, indicating a small number of carbon-oxygen functional groups. More information regarding carbon-oxygen functional groups were provided by analyzing the O1s (Fig. 1E). The C=O (532.5 eV) and C–O (533.9 eV) are well defined but slightly superimposed. The atomic compositions of C and O were calculated to be 94.6% and 5.4%, respectively. The characterized carbon-oxygen functional groups resulted in oxygenated defects in graphene, which might subsequently affect the conductivity of the graphene layer. However, the acquired enhanced performance of the PEC biosensor demonstrated the influence of such amount of introduced defects was acceptable.

3.2. Characterization of rGO/ZnO based photoanode

The FE-SEM image of ZnO NRs array is shown in Fig. 2A and B. The individual ZnO NRs grew uniformly all over the surface of the substrate, with the rod diameter around 100 nm. Most of the NRs stood vertically to the substrate, while some of them grew at a tilted angle due to the partially nonuniform ZnO seed layer formed on the wrinkled graphene layer (Choi et al., 2011). Fig. 2C shows the high resolution (HR) TEM image of the ZnO NR grown on rGO, which indicates the single-crystalline of NR. The spacing between adjacent lattice planes in the ZnO was 0.26 nm, demonstrating the preferential growth of ZnO NRs along the [0001] *c*-axis orientation. In the Raman spectrum (Fig. 2E), in addition to the D and G bands of rGO, another two peaks around 98 cm^{-1} and 438 cm^{-1} are corresponding to the E_2^{low} and E_2^{high} mode of the ZnO NRs array. The results confirm the successful integration of the ZnO NRs and the rGO. In the XRD pattern of the composite structure (Fig. 2F), an intense diffraction peak at $2\theta=34.42°$ is observed because of the (0002) plane of ZnO. A clear peak at $2\theta=26.42°$ is observed as well, which is derived from the (0002) plane of graphene. The rest of the peaks are assigned to the hexagonal phase wurtzite ZnO (JCPDS no. 89-0511) and the FTO substrate. Therefore, the results further demonstrate the realization of direct growth of well-orientated ZnO NRs array onto the rGO layer.

3.3. PEC property of rGO/ZnO based photoanode

Electrochemical impedance spectroscopy (EIS) was carried out with or without UV illumination at bias potential of 0 V vs. Ag/AgCl. The semicircle in the Nyquist plot at high frequencies is the characteristic of the charge transport process, and the diameter of the semicircle is equal to the charge transfer resistance (R_{ct}). As shown in Fig. 3A, the rGO/ZnO sample has the smallest semicircle diameter in the condition of UV illumination, indicating a more effective separation of photoinduced electron–hole pairs and faster charge transport process under UV illumination compared to the pristine ZnO NRs array. Thus, the enhanced PEC performance of rGO/ZnO heterostructure has been demonstrated.

PEC behaviors of pristine ZnO NRs array and rGO/ZnO NRs array heterostructure with and without addition of GSH at bias potential of 0 V vs. Ag/AgCl were also shown in Fig. 3B. No photocurrent was observed in the dark. When the UV illumination was applied, the photocurrent was composed of three stages: (i) the photocurrent climbed promptly, (ii) the photocurrent decreased sharply, and (iii)

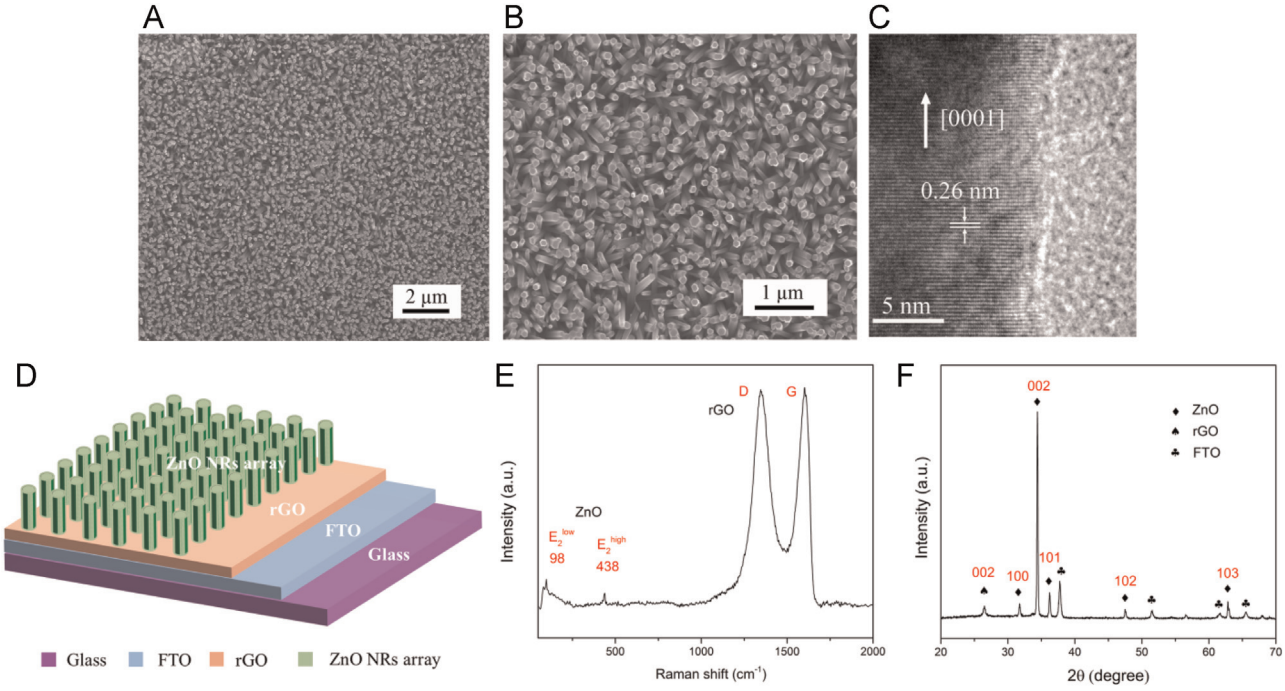

Fig. 2. (A) and (B) SEM images of the ZnO NRs array grown on the rGO layer at different magnifications; (C) TEM image of the single ZnO NR which was detached from the NRs array by sonication and transferred on the TEM grid; (D) schematic of the fabricated rGO/ZnO NRs array heterostructure as a photoanode; (E) Raman spectrum and (F) XRD pattern of the fabricated rGO/ZnO NRs array heterostructure.

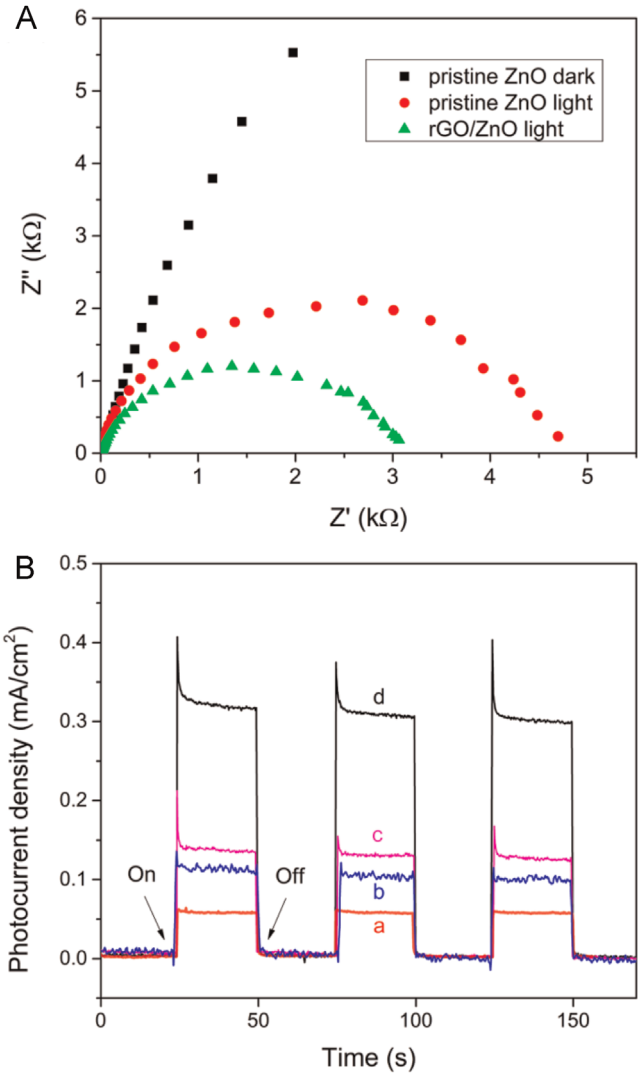

Fig. 3. (A) EIS Nyquist plots of pristine ZnO NRs array and rGO/ZnO NRs array heterostructure in the dark or under UV illumination in 0.1 M PBS at bias potential of 0 V vs. Ag/AgCl. (B) Photoresponse of pristine ZnO NRs array in(a) 0.1 M PBS and (b) 0.1 M PBS containing 15 μM GSH, and rGO/ZnO NRs array heterostructure in (c) 0.1 M PBS and (d) 0.1 M PBS containing 15 μM GSH at bias potential of 0 V vs. Ag/AgCl.

the photocurrent gradually reached a stable state. These three steps are associated with the photogenerated electrons under UV irradiation, the recombination of photogenerated electron–hole pairs, and the balance of generation and recombination of electron–hole pairs, respectively (Wang et al., 2013). The pristine ZnO NRs array electrode showed an average photocurrent density of 0.07 mA/cm^2 (curve a), whereas the rGO/ZnO electrode performed an average photocurrent density of 0.15 mA/cm^2 with a 114% increase (curve c), indicating the remarkable improvement of the photocurrent conversion efficiency of ZnO NRs array by the introduction of the rGO layer between ZnO and FTO electrode. There is no doubt that when a positive bias potential is applied, the photocurrent density will apparently increase due to the greater charge separation and longer lifetime of photogenerated electron–hole pairs. Neverthless, in order to realize the self-powered device and take the selectivity of the PEC biosensor into consideration, bias potential of 0 V was selected in this work.

Since GSH plays an important role in many biological functions, it was adopted as a model molecule to demonstrate the feasibility of fabricating a rGO/ZnO based PEC biosensor. When GSH was added in the blank PBS (15 μM), it acted as an effective electron

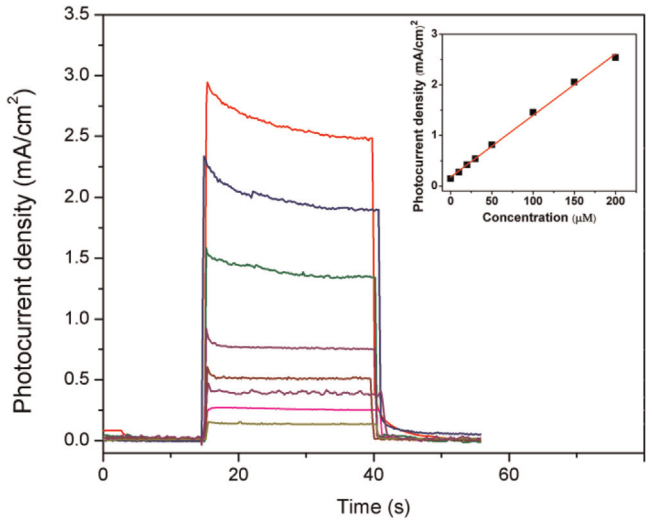

Fig. 4. Photocurrent responses of rGO/ZnO based photoanode in 0.1 M PBS in the presence of 0, 10, 20, 30, 50, 100, 150, 200 μM GSH (from bottom to top) at 0 V (vs. Ag/AgCl) with UV irradiation. Inset: linear calibration curve.

donor for scavenging the photogenerated holes at the surface of ZnO and thus inhibiting the electron–hole recombination. Therefore, the photocurrent density was further strengthened for both pristine ZnO (curve b) and rGO/ZnO (curve d) electrodes in Fig. 3B. Because of the more significant photocurrent change for rGO/ZnO electrode with presence of GSH, such heterostructure is more suitable for the sensitive monitoring of GSH concentration.

3.4. PEC biosensing of GSH

For further biosensing of GSH, Fig. 4 demonstrates the time-based photocurrent response of the rGO/ZnO based photoanode in the presence of GSH with various concentrations at an applied potential of 0 V (vs. Ag/AgCl) under UV illumination. The photocurrent density performed a fine linear relationship with the concentration of GSH from 10 to 200 μM (R^2=0.997). This is wider than that of other PEC biosensing methods based on flower-like Cu_2O/ZnO (Li et al., 2014), porous TiO_2–Pt nanowhisker (Chen et al., 2012) and IrO_2–Hemin–TiO_2 (Tang et al., 2013), as well as electrochemical biosensing methods based on Hg/Pd (Antwi et al., 2011), ordered mesoporous carbon electrode (Ndamanisha et al., 2009) and $Cu(OH)_2$–carbon ionic liquid electrode (Safavi et al., 2009). The detection limit was estimated at 2.17 μM using 3σ, which is lower than that of PEC methods based on graphene–CdS nanocomposites (Zhao et al., 2012), electrochemical method based on Hg/Pd electrode (Antwi et al., 2011), and electrochemiluminescence method based on CdTe quantum dots-graphene oxide (Wang et al., 2009). The detailed performance comparisons with previously reported literatures about GSH biosensing are listed in Table S1. Obviously, the proposed rGO/ZnO based PEC biosensor shows promise for applications in the simple monitoring of GSH with high sensitivity and relatively wide linear range.

The mechanism responsible for the elevated PEC biosensing performance is the step-wise energy band structure constructed when rGO is in combination with ZnO and FTO, as shown in Scheme 1. The photogenerated electrons are favorable to transport from the conduction band of ZnO to the FTO through the rGO layer because of the relevant band positions of each component. This process effectively suppresses the charge recombination. On the other hand, the photogenerated holes are easier to transport from the valence band of ZnO to the surface of ZnO nanostructure, and subsequently take part in the oxidation of GSH to glutathione disulfide (GSSG). As a result, even with a bias potential of 0 V, the

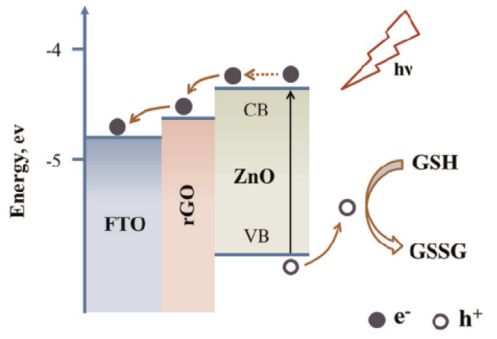

Scheme 1. Illustration of the PEC mechanism for GSH biosensing at graphene/ZnO NRs array based photoanode. CB and VB are the conduction band and valence band, respectively.

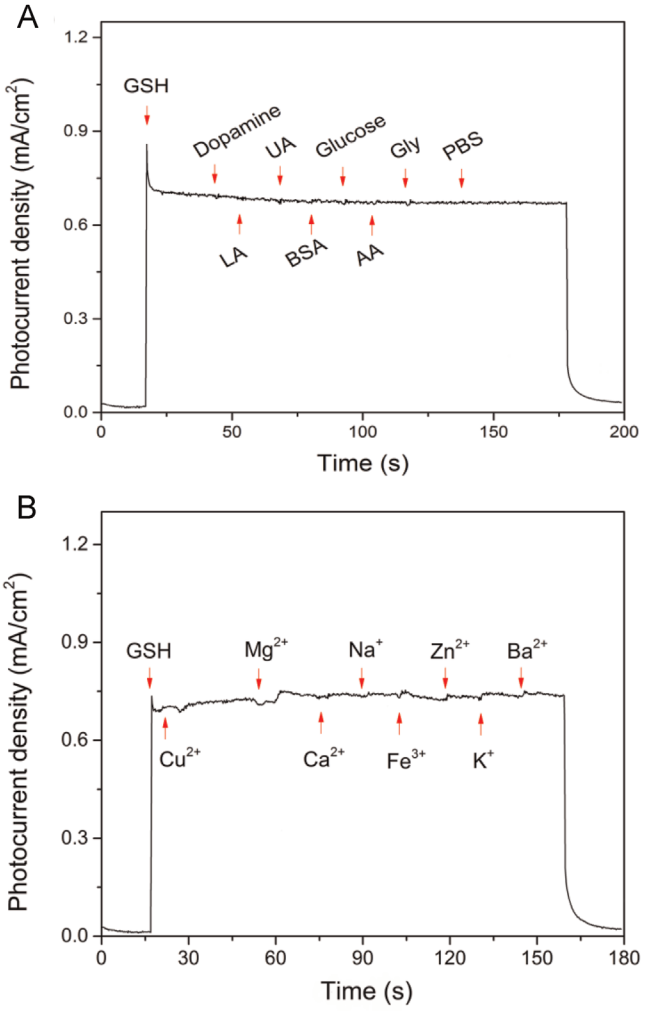

Fig. 5. Photocurrent response of the rGO/ZnO based PEC biosensor at 0 V bias (vs. Ag/AgCl) in the presence of GSH (50 μM) and (A): dopamine, LA, UA, BSA, glucose, AA, Gly with the concentration of 20 μM and PBS, as well as (B): various metal ions such as Cu^{2+}, Mg^{2+}, Ca^{2+}, Na^{+}, Fe^{3+}, Zn^{2+}, K^{+} and Ba^{2+} with the concentration of 20 μM.

efficient separation of photoinduced charge carriers was realized to finally achieve a self-powered PEC biosensor.

3.5. Selectivity, reproducibility and stability

The selectivity of the rGO/ZnO based PEC sensor is confirmed by measuring the photocurrent response for common chemical or biological interferences as well as various metal ions with the concentration of 20 μM, showing much smaller or negligible signals compared to that of GSH with the concentration of 50 μM (Fig. 5A and B). The excellent selectivity is attributed to the fact that the low applied bias potential minimizes the interference of other reductive species (Tang et al. 2013; Tu et al., 2010). Moreover, the relative standard deviation (R.S.D) of the photoresponse to 50 μM GSH was 4.5% for six successive measurements. The R.S.D for detection of 50 μM GSH with six different rGO/ZnO based photoanodes under the same condition was 6.7%. Additionally, the time-dependent photoresponse measurement of the rGO/ZnO NRs array shows the photocurrent density was highly stable for more than 2 h (Fig. S1A). Also, the repeating test of the fabricated PEC biosensor for over a half month confirmed that over 90% of the initial photocurrent response was maintained (Fig. S1B), indicating the structural stability of the fabricated photoanode and its practical potential for biosensing experiments.

4. Conclusions

In summary, we have realized the direct synthesis of ZnO NRs array on rGO layer and demonstrated the enhanced PEC property of the rGO/ZnO based photoanode under UV irradiation. Such enhancement was attributed to the fact that the introduction of rGO layer between FTO and ZnO NRs array resulted in a favorable energy band structure and significantly facilitated the electron migration to the electrode. Thus, the separation of photoinduced charge was efficiently improved. Subsequently, such nanostructure was successfully adopted for self-powered PEC biosensing of GSH at 0 V bias, with a linear range from 10 μM to 200 μM and a detection limit of 2.17 μM. Moreover, the fabricated PEC biosensor performed excellent selectivity, reproducibility and stability, suggesting the rGO/ZnO nanostructure is a competitive candidate for construction of other novel PEC biosensors.

Acknowledgments

This work was supported by the National Major Research Program of China (2013CB932600), Major Project of International Cooperation and Exchanges (2012DFA50990), the Program of Introducing Talents of Discipline to Universities, the National Natural Science Foundation of China (51232001, 51172022, 51372023), the Research Fund of Co-construction Program from Beijing Municipal Commission of Education, the Fundamental Research Funds for the Central Universities, the Program for Changjiang Scholars and Innovative Research Team in University.

Appendix A. Supplementary material

Supplementary data associated with this article can be found in the online version at http://dx.doi.org/10.1016/j.bios.2014.09.055.

References

Antwi, C., Johnson, A.S., Selimovic, A., Martin, R.S., 2011. Anal. Methods 3, 1072–1078.
Chang, H., Sun, Z., Ho, K.Y.-F., Tao, X., Yan, F., Kwok, W.-M., Zheng, Z., 2011. Nanoscale 3, 258–264.
Chen, G., Wang, J., Wu, C., Li, C.-z., Jiang, H., Wang, X., 2012. Langmuir 28, 12393–12399.
Choi, W.M., Shin, K.-S., Lee, H.S., Choi, D., Kim, K., Shin, H.-J., Yoon, S.-M., Choi, J.-Y., Kim, S.-W., 2011. Nano Res. 4, 440–447.
Fan, Z., Wang, K., Wei, T., Yan, J., Song, L., Shao, B., 2010. Carbon 48, 1686–1689.
Geim, A.K., Novoselov, K.S., 2007. Nat. Mater. 6, 183–191.
Hendry, E., Koeberg, M., O'Regan, B., Bonn, M., 2006. Nano Lett. 6, 755–759.

Hu, Y., Xue, Z., He, H., Ai, R., Liu, X., Lu, X., 2013. Biosens. Bioelectron. 47, 45–49.
Kaidashev, E.M., Lorenz, M., von Wenckstern, H., Rahm, A., Semmelhack, H.-C., Han, K.-H., Benndorf, G., Bundesmann, C., Hochmuth, H., Grundmann, M., 2003. Appl. Phys. Lett. 82, 3901–3903.
Kumar, B., Lee, K.Y., Park, H.-K., Chae, S.J., Lee, Y.H., Kim, S.-W., 2011. ACS Nano 5, 4197–4204.
Li, J., Li, H., Xue, Y., Fang, H., Wang, W., 2014. Sens. Actuators B: Chem. 191, 619–624.
Liang, M., Jia, S., Zhu, S., Guo, L.-H., 2008. Environ. Sci. Technol. 42, 635–639.
Liu, F., Zhang, Y., Yu, J., Wang, S., Ge, S., Song, X., 2014. Biosens. Bioelectron. 51, 413–420.
Liu, J., Lu, R., Xu, G., Wu, J., Thapa, P., Moore, D., 2013. Adv. Funct. Mater. 23, 4941–4948.
Ndamanisha, J.C., Bai, J., Qi, B., Guo, L., 2009. Anal. Biochem. 386, 79–84.
Safavi, A., Maleki, N., Farjami, E., Mahyari, F.A., 2009. Anal. Chem. 81, 7538–7543.
Tang, J., Kong, B., Wang, Y., Xu, M., Wang, Y., Wu, H., Zheng, G., 2013. Nano Lett. 13, 5350–5354.
Tang, J., Wang, Y., Li, J., Da, P., Geng, J., Zheng, G., 2014. J. Mater. Chem. A 2, 6153–6157.
Tu, W., Dong, Y., Lei, J., Ju, H., 2010. Anal. Chem. 82, 8711–8716.
Wang, M., Sun, L., Lin, Z., Cai, J., Xie, K., Lin, C., 2013. Energy Environ. Sci. 6, 1211–1220.
Wang, Y., Lu, J., Tang, L., Chang, H., Li, J., 2009. Anal. Chem. 81, 9710–9715.
Yan, K., Wang, R., Zhang, J., 2014. Biosens. Bioelectron. 53, 301–304.
Yang, D., Velamakanni, A., Bozoklu, G., Park, S., Stoller, M., Piner, R.D., Stankovich, S., Jung, I., Field, D.A., Ventrice Jr, C.A., Ruoff, R.S., 2009a. Carbon 47, 145–152.
Yang, X., Wolcott, A., Wang, G., Sobo, A., Fitzmorris, R.C., Qian, F., Zhang, J.Z., Li, Y., 2009b. Nano Lett.ers 9, 2331–2336.
Yue, H.Y., Huang, S., Chang, J., Heo, C., Yao, F., Adhikari, S., Gunes, F., Liu, L.C., Lee, T. H., Oh, E.S., 2014. ACS Nano 8, 1639–1646.
Zhan, W.-W., Kuang, Q., Zhou, J.-Z., Kong, X.-J., Xie, Z.-X., Zheng, L.-S., 2013. J. Am. Chem. Soc. 135, 1926–1933.
Zhang, X., Li, S., Jin, X., Zhang, S., 2011. Chem. Commun. 47, 4929–4931.
Zhang, X., Liao, Q., Chu, M., Liu, S., Zhang, Y., 2014. Biosens. Bioelectron. 52, 281–287.
Zhang, X., Zhang, Y., Liao, Q., Song, Y., Ma, S., 2013. Small 23, 4045–4050.
Zhang, Y., Yan, X., Yang, Y., Huang, Y., Liao, Q., Qi, J., 2012. Adv. Mater. 24, 4647–4655.
Zhao, W.-W., Liu, Z., Shan, S., Zhang, W.-W., Wang, J., Ma, Z.-Y., Xu, J.-J., Chen, H.-Y., 2014. Sci. Rep. 4, 4426–4431.
Zhao, X., Zhou, S., Shen, Q., Jiang, L.-P., Zhu, J.-J., 2012. Analyst 137, 3697–3703.